Adv. Nat. Sci.: Nanosci. Nanotechnol. **11** (2020) 045003 (10pp) https://doi.org/10.1088/2043-6254/abb93b

Hierarchical mesoscale assembly of PbO_2 on 3D titanium felt/TiO_2 nanotubular array electrode for anodic decolourisation of RB-5 dye

C Harito[1], S Z J Zaidi[2], D V Bavykin[2], A S Martins[2,3], B Yuliarto[4,5], F C Walsh[2] and C Ponce de León[2]

[1] Industrial Engineering Department, Faculty of Engineering, Bina Nusantara University, 11480 Jakarta, Indonesia
[2] Energy Technology Research Group, Faculty of Engineering and Physical Sciences, University of Southampton, SO17 1BJ, Southampton, United Kingdom
[3] National Institute of Alternative Technologies for Detection, Toxicological Evaluation and Removal of Micropollutants and Radioactive Substances (INCT-DATREM), Institute of Chemistry, São Paulo State University, Araraquara, 14800–900, São Paulo, Brazil
[4] Advanced Functional Materials (AFM) Laboratory, Engineering Physics, Institut Teknologi Bandung, 40132, Bandung, Indonesia
[5] Research Center for Nanosciences and Nanotechnology (RCNN), Institut Teknologi Bandung, 40132, Bandung, Indonesia

E-mail: christian.harito@binus.ac.id

Received 11 April 2020
Accepted for publication 7 June 2020
Published 24 September 2020

Abstract

Hierarchical PbO_2 nanoparticles (NPs) were grown by hydrothermal method on TiO_2 nanotubes (NTs) at 3D titanium felt, which is simple and scalable method. TiO_2 NTs were formed on titanium felt by anodising at 25 °C in environmentally friendly methanesulphonic acid solution. The growth of PbO_2 on the TiO_2 NTs depended on immersion time during hydrothermal synthesis and followed a LaMer-Dinegar burst kinetic model of nucleation and growth. PbO_2 formation began with rapid nucleation, followed by mesoscale assembly due to organic capping of poly(vinylpyrrolidinone). The electrochemical performance of 3D electrode was recorded in pH 3 sodium sulphate solutions containing Reactive Black 5 (RB-5) azo dye at 25 °C. The resulting hierarchical 3D electrode achieved 98% decolourisation after 50 min of anodic oxidation with a first order batch decay rate of 0.0875 min^{-1}.

Keywords: 3D electrode, electrocatalyst, hierarchical, lead dioxide, TiO_2 nanotube
Classification numbers: 2.00, 4.00, 5.06, 5.11, 5.12

1. Introduction

In recent years, degradation of organic matter residue (OMR) in solution by anodic oxidation has been used to treat wastewater. New electrocatalysts and supports are needed to improve the process efficiency and there is a need to develop low-cost materials which remain stable during the electrochemical water treatment [1]. Research has centred on materials that are effective for generation of active oxidising species with sufficient electrical conductivity and a high electrocatalytic activity for *in-situ* generation of oxidants, notably hydroxyl radicals. Due to their unique architecture, hierarchical 3D electrodes offer improvements over conventional electrodes in providing extensive active sites [2], better electrolyte infiltration and ease of bubble release [3]. The hierarchical architecture of composite electrode has been exploited in water splitting [4], energy storage such as flow batteries [5], and industrial catalyst [6]. The increasing

interest in hierarchical electrodes signifies efficient design and applications have diversified in electrocatalysis.

The use of titanium as an electrode has been reported due to its moderate cost, robustness, acceptable electrical conductivity and chemical stability [7]. Titanium can form a surface oxide layer which can be functionalised and provides corrosion protection. Under certain conditions, titanium oxides can act as photocatalysts [8], composite coatings [9, 10], sensors [11, 12], antibacterial surfaces [13] and ionic diodes [14]. In addition to the above properties, TiO_2 provides hydrophilicity during deposition of metal oxides such as PbO_2 from aqueous solution. The use of TiO_2 coated electrodes is restricted due to the possibility of passivation and limited electrocatalytic activity for electrooxidation of organic compounds. Over the last two decades, it has been recognised that the electrocatalytic properties can be enhanced by the presence of active and unreactive materials, making it feasible to achieve catalytically active oxide coatings, such as Cu_2O, PbO_2 [1, 15, 16].

PbO_2 can be deposited over nanoparticles, achieving a practical, low cost electrode for environmental remediation of wastewater. Contemporary research has revealed that the synthesis of PbO_2 decorated TiO_2 nanotubular arrays can achieve complete mineralisation of Reactive Blue-194 at a current density of 150 $mA.cm^{-2}$ [17]. PbO_2 coatings were typically achieved by electrodeposition [18]. The hydrothermal method which is simple and scalable was used in this study. TiO_2 nanotubular arrays can be grown by anodising pure titanium sheets, providing an active support for the deposition of electroactive species, such as PbO_2. PbO_2 is particularly the most attractive oxide for electrochemical water treatment with an approximate electrical conductivity of $2.5 \times 10^3\ \Omega^{-1}\ cm^{-1}$ [19].

In this work, titanium felt was anodised in fluoride-containing aqueous methanesulphonic acid (MSA) electrolytes under controlled operating conditions to grow TiO_2 nanotubes (NTs) which were then decorated with PbO_2 by immersion and hydrothermal treatment to produce a novel 3D coating having applications in electrocatalytic degradation of Reactive Black 5 (RB-5) dye. Due to its water solubility and its ability to produce a covalent bond with fibre, RB-5 dye is commonly used in textile industry [20]. The results provide important information on interfacial surface transitions between TiO_2 and PbO_2 layers.

2. Experimental details

Reagent grade 70% methanesulphonic acid (MSA), ammonium fluoride, ammonium persulphate, 99% oxalic acid, poly (vinylpyrrolidinone) (PVP, relative molar mass = 55000) and Reactive Black 5 dye were obtained from Sigma Aldrich, while lead nitrate, sodium hydroxide, sulphuric acid, sodium hydroxide, sodium sulphate, ethanol (98%) and acetone were obtained from Fischer Scientific and used as received.

2.1. Anodising of titanium felt

The Ti felt (NV Bekaert SA) was pre-treated in a 10 wt.% oxalic acid solution at 70 °C for 20 min. The Ti felt was washed with ethanol and deionised water, then dried overnight at 90 °C in air. Anodising was carried out in an undivided glass cell of 100 cm^3 volume. The Ti felt was connected as an anode with dimensions of 2 cm × 2 cm × 0.15 cm. A graphite plate of 1.5 cm × 6 cm × 1.2 cm dimensions was used as a cathode. The electrolyte was magnetically stirred at 300 rev min^{-1} using a 0.06 cm diameter, 0.25 cm long PTFE-coated steel, cylindrical stirring bar (Fischer Scientific). The Ti felt was anodised in 1 M MSA electrolyte containing 1 wt.% ammonium fluoride. The anode and cathode were separated at 1 cm apart and applied a cell potential difference of 10 V and 20 V for 1 h at 25 °C.

2.2. Synthesis of lead dioxide

The PbO_2 was deposited hydrothermally in the presence of PVP as a catalyst support, which served as a structure directing agent. 0.015 M $Pb(NO_3)_2$ and 1 M NaOH were mixed at 25 °C. 0.1 g of PVP was added to 75 cm^3 of the above mixture and allowed to stir overnight until complete dissolution has taken place. 3 cm^3 of 1.5 M $(NH_4)_2S_2O_8$ was dissolved in the resultant solution, transferred to an autoclave and heated at 60 °C with samples of Ti felt/TiO_2 NTs for 1 min, 5 min, 15 min, 6 h, and 12 h. The resultant samples were cooled down overnight, to produce an adherent PbO_2 coating on the substrate.

2.3. Heat treatment or calcination

The resulting Ti felt/TiO_2 NTs/PbO_2 composite samples were annealed at 450 °C for 1 h in air using an electric furnace. The calcined samples were later used in decolourisation studies.

2.4. Characterisation of coated substrate

A field emission scanning electron microscope (FESEM, JEOL 6500F) was used to characterise all anodised samples. A Raman confocal microscope (Renishaw, RM 2000) was used to obtain Raman spectra employing light source of 632.8 nm wavelength with 10% laser intensity. The exposure time was approximately 30 s. A Rigaku SmartLab x-ray diffractometer (XRD) operated at 9 kW with Cu target was used for phase characterisation.

2.5. Electrochemical experiments

The electrochemical studies were accomplished by using computer aided PGSTAT302N potentiostat/galvanostat from Autolab (Eco Chemie, Netherlands) utilising Nova 1.11 software. All samples (Ti felt, Ti felt/TiO_2 NTs, and Ti felt/TiO_2 NTs/PbO_2) were used as an anode for electrochemical discolouration of RB-5 dye. A 100 cm^3 solution containing 20 ppm of RB-5 dye in 0.5 M sodium sulphate as a background electrolyte was electrolysed at a constant potential 1.5 V versus Hg/HgO (0.6 M NaOH) at pH 3 and 25 °C.

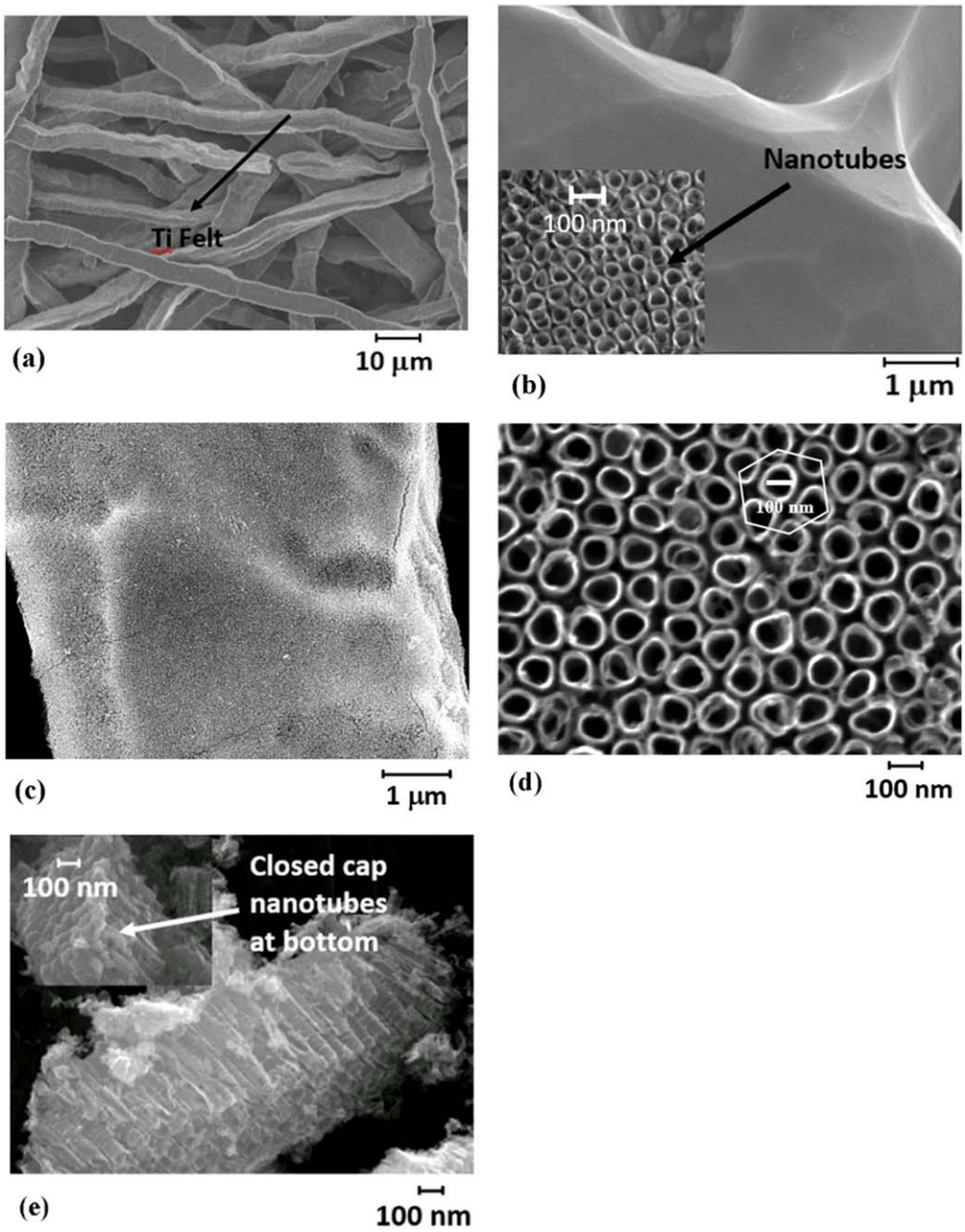

Figure 1. SEM images of nanotubes on the titanium felt substrate obtained by anodising: (a) Pre-treated Ti felt substrate; (b) TiO_2 NTs on Ti felt at 10 V, 1 wt.% NH_4F, 1 M MSA, the inset shows the TiO_2 NTs at higher magnification; (c) TiO_2 NTs on Ti felt at 20 V, 1 wt.% NH_4F, 1 M MSA; (d) at higher magnification; (e) Pore length of figure (c) sample at cross sectional view of mechanically scratched nanotubes, the inset shows the closed capped nanotubes from the bottom.

The pH of the electrolyte was stable throughout the electrochemical studies. Platinum mesh (1.5 cm × 1.5 cm) and mercury/mercuric oxide (Hg/HgO in 1.0 M NaOH) were used as a counter and reference electrode respectively.

3. Results and discussion

3.1. Surface characterisation of TiO_2 nanotubes

Morphological and elemental analysis of the titanium felt was conducted by means of SEM and EDX, as shown in figures 1(a)–(e). Surface TiO_2 NTs were achieved by anodising Ti felt which was pre-treated with oxalic acid at 80 °C for 20 min SEM images of pre-treated Ti felt (figure 1(a)) and hierarchical nanotube arrays on anodised Ti felt (figure 1(b)) reveal that the NTs have a hexagonal pattern with a smooth surface as reported in literature [21]. The NTs have a vertical arrangement of close packed NTs.

TiO_2 NTs can act as nucleation site and container of nanostructures, so it is feasible to decorate each anodised nanotube with an oxygen transferring metal oxide, such as PbO_2. The formation of TiO_2 NTs on 3D Ti felt can be observed in the SEM images (figures 1(b)−(d)). The images

Table 1. Comparison of discolouration rate by TiO_2 and PbO_2 for degradation of model dye from selected literature.

Method/type of dyes	Parameters and conditions	k/min^{-1}	Colour removal/ %	Time/min	References
Anodic oxidation of methyl orange	P25 TiO_2/PbO_2, pH 2.5, E_{anode} 1.5 V versus Ag/AgCl/saturated KCl	—	66.4	120	[27]
Anodic oxidation of Acid Blue 113	Pb/PbO_2, current density $j = 60$ mA cm^{-1}, 25 °C	—	93.6	360	[28]
Anodic oxidation of Acid Blue 113	$Ti/TiO_2/PbO_2$ disc electrode, $j = 60$ mA cm^{-1}, 25 °C	—	98	60	[28]
Anodic oxidation of Acid Red 27	Stainless steel/PbO_2, pH 2, current density $j = 20$ mA cm^{-1}, 25 °C	0.0575	97	300	[29]
Anodic oxidation of Reactive Black 5	RVC/TiO_2 nanosheets/PbO_2, pH 3, $E = 2.5$ V versus Hg/HgO, current density, $j = 2$ mA cm^{-1}, 25 °C	0.060	98	60	[30]
Anodic oxidation of Reactive Black 5	3D Ti felt, $E = 1.5$ V versus Hg/HgO, pH = 3, 25 °C	0.0012	7	60	This study
Anodic oxidation of Reactive Black 5	3D Ti felt/TiO_2 nanotubes, $E = 1.5$ V versus Hg/HgO, pH = 3, 25 °C	0.0058	36	60	This study
Anodic oxidation of Reactive Black 5	3D calcined Ti felt/TiO_2 nanotubes/PbO_2 ($t_i = 12$ h) $E = 1.5$ V versus Hg/HgO, pH = 3, 25 °C	0.0875	98	50	This study

also showed that the Ti NTs were dispersed uniformly on the Ti felt. The Ti felt anodised at a cell voltage of 20 V appeared darker in colour, due to the longer TiO_2 NTs formed. It is noticeable that the diameter of nanotubes produced using a cell voltage of 20 V (figures 1(c), (d)) was ~100 nm which was larger than samples anodised at a cell voltage of 10 V with ~50 nm in diameter (figure 1(b)). Pore widening in the nanotubular array could be controlled by adjusting the potential distribution over the 3D electrode. The nanotubes produced at a cell voltage of 20 V for 1 h showed a close packed, vertical arrangement with a length ~230 nm and a closed cap at the bottom of the nanotubes (figure 1(e)), which was in agreement with our previous work on 2D Ti foil [22].

The surface of anodised felt contains uniform films. The formation of ordered nanotubes is due to the presence of fluoride ions as reported [23, 24]. The fluoride ion can be used in the form of sodium fluoride, ammonium fluoride or hydrofluoric acid, we preferred the ammonium salt for relative safety in handling.

The mechanism is related to the electrochemical development of oxide layer on the Ti felt substrate according to the following reaction:

$$Ti + H_2O \rightarrow TiO_2 + 4H^+ + 4e^-, \quad (1)$$

and subsequent dissolution with fluoride ions [25, 26]:

$$TiO_2 + 6F^- + 4H^+ \rightarrow TiF_6^{2-} + 2H_2O. \quad (2)$$

Initially, anodising forms a dense layer of TiO_2 on the Ti felt substrate. In the presence of ammonium fluoride, the TiO_2 film can dissolve, forming an anionic fluorotitanate complex. Fluoride ion migration is controlled by the potential gradient, leading to selective dissolution and formation of an ordered array of nanotubes. The oxide layer dissolves at the pore mouth and oxide formation held at the bottom pores. The nanotubular structure separates from the substrate due to the barrier layer of residual oxide. This compact layer of nanotubes depends upon factors such as acid concentration, fluoride ion intake and applied potential [26], as shown in table 1.

3.2. Decoration of TiO_2 nanotubes with PbO_2

The nanotubular arrangement of TiO_2 NTs is more hydrophilic in nature compared to Ti metal. Therefore, these modified surfaces are able to take in liquid and absorb the aqueous phase inside the TiO_2 NTs on immersion to a solution. This wetting characteristic enables filling of the tubes with aqueous solution of lead nitrate as metal source, ammonium sulphate as oxidant and PVP as a structure directing agent of PbO_2 [31]. Hence, PbO_2 accumulates on the TiO_2 NTs grew over the surface of the Ti felt on immersion during hydrothermal treatment in figures 2(a)–(d).

The deposition of PbO_2 on nanotubular arrangement on Ti felt was proved by Raman and FESEM studies. Figures 2(a)–(c) reveals SEM images for a deposited lead dioxide during 1, 5, and 15 min of immersion on the TiO_2 NTs, which showed rapid nucleation of PbO_2 NPs in which the surfaces of 3D felt have been concealed at 15 min (figures 2(c), 3(a) and (b)). Some of the uncovered nanotubes can still be seen at low immersion times (e.g. 1 and 5 min) in figures 2(a), (b). The quantity of deposited PbO_2 in the nanotube arrays could be increased by tuning the immersion time. The surface coverage was approximately improved from 20%, 60% to 90% respectively for 1, 5, and 15 min of immersion. In the first one minute, the precursors went into the pores of nanotubes, followed by nucleation over the top of nanotubes due to larger size of PbO_2 compared to TiO_2 NTs. The PbO_2 NPs have an oval shape of approximately 100 nm, showing monodispersed spontaneous nucleation at hydrothermal temperature of 60 °C. The kinetics of spontaneous nucleation may be controlled by adjusting temperature, the concentration of precursors and the strength of oxidising agent, i.e., ammonium persulphate, as postulated by LaMer-Dinegar [32].

The LaMer-Dinegar theory could be applied for colloidal monodispersed condition which was used to predict further crystal growth (figure 2(d)). In this case, the PVP was used as a surface directing agent [31] which capped the surface of PbO_2 restricting further growth. The negatively charged PVP then acted as new nucleation centres of Pb^{2+} ions, resulting in local aggregation of nanoparticles in figures 3(c), (d). This aggregation resembled diffusion-controlled growth in LaMer-Dinegar theory with assisted aggregation due to the structure direction and interlinking bridges by PVP [32]. Lead oxide and PVP became inorganic-organic building block of spherical mesocrystal formation. This non-classical crystallisation usually leads to high surface area functional materials [33, 34]. Coalescence of microspheres occurred at long reaction times since the space for growth was limited in figures 3(e) and (f). PVP continued to maintain the particle size of PbO_2 as shown in the inset of figure 3(f). The decoration of nanotubes with PbO_2 on the nanotubular arrays over Ti felt substrate was expected to increase the electrochemical properties of the coating.

EDX elemental analysis is shown in figure 4 for this coating. The surface contained lead in abundance with titanium and traces of oxygen. This is consistent with uniform adhesion of PbO_2 over the Ti felt strands. However, EDX did not show stoichiometric phases of TiO_2 and PbO_2 due to interference from the Ti felt substrate. Raman spectroscopy revealed the structural properties of coatings related to the presence of PbO_2 and formation of anatase phase after annealing as shown in figure 5(a). The distinct Raman peaks were observed at 428 cm^{-1} and 137 cm^{-1} which showed the presence of PbO_2 [35] and the effect of annealing in transforming the substrate to anatase phase, as indicated by previous research [36]. In figure 5(a), no significant anatase peaks were observed before calcination, showing that the hydrothermal synthesis of PbO_2 at 60 °C did not significantly affect the structure of the titanium phase. The anatase phase of the calcined Ti/TiO_2 NTs was also confirmed by XRD in figure 5(b).

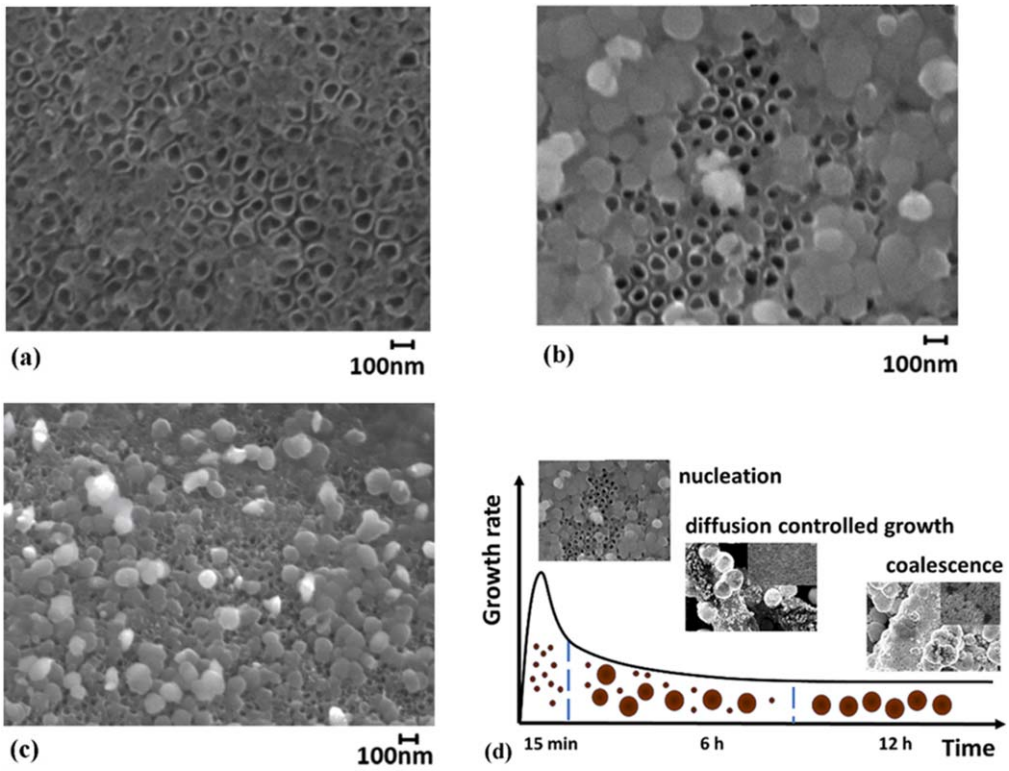

Figure 2 FESEM images of the nucleation stage of PbO_2 on 3D Ti felt/TiO_2 NTs electrode by hydrothermal treatment with several immersion times: (a) immersion time (t_i) = 1 min; (b) t_i = 5 min; (c) t_i = 15 min; (d) the stages of PbO_2 growth are projected to LaMer-Dinegar burst model.

3.3. Electrochemical studies of novel coatings containing PbO_2

The nanotubes coated with PbO_2 NPs on a Ti felt substrate are shown in figure 3(f). The 12 h immersion time was used since it contained the most PbO_2 after nucleation and growth in figure 2(d). Such surfaces are suitable for use in the anodic oxidation of RB-5 dye. Linear sweep voltammetry was used to examine the electrochemical characteristics of Ti felt/TiO_2 nanotubes and Ti felt/TiO_2 NTs/PbO_2 electrodes towards RB-5 dye. The main goal of these studies was to detect the electrocatalytic performance towards oxidation of organic molecules and to know the potential at which oxygen evolution began.

Figure 6 shows the polarisation curve obtained in the overpotential range from 0.4 V to 2.0 V versus [Hg/HgO] NaOH (sat.) at a sweep rate of 10 mV s^{-1}, in 0.6 dm^3 volume solution containing 20 × 10^{-5} M (20 ppm) of RB-5 dye at pH 3 with 0.5 M Na_2SO_4 in a working electrode compartment while counter electrode containing only 0.5 M of Na_2SO_4 at pH 3. The scan towards more positive potentials showed a steep rise in anodic current, corresponding to decomposition of RB-5 azo dye into oxygenated products and intermediates, attributed to oxygen evolution and other anodic reactions. This conversion of organic pollutant (RB-5 dye) to oxygenated products was interceded by $^{\cdot}OH$ free radical produced at a non-active anode surface due to primary water discharge over Ti felt/TiO_2 NTs/PbO_2 electrode surfaces. The oxidation peak in voltammogram indicates oxidative degradation of dye at anode via *in-situ* $^{\cdot}OH$ mediation. In case of Ti felt/TiO_2 NTs/PbO_2 coatings, oxygen evolution started at a potential of 1.5 V versus Hg/HgO (0.6 M NaOH) at a scan rate of 10 mV s^{-1}. This corresponds to the most positive potential before anodic oxidation of dye takes place as a primary reaction, followed by the secondary reaction of oxygen evolution at more positive potentials. For Ti felt/TiO_2 NTs, oxygen evolution took place at 1.0 V versus Hg/HgO due to water electrolysis at anode [37]. Ti felt/TiO_2 NTs/PbO_2 surfaces showed electrocatalytic activity for anodic oxidation of RB-5 dye at 1.5 V versus Hg/HgO. Previous reports indicated that mediated $^{\cdot}OH$ radicals produced via water discharge act as highly active oxidants and negligible adsorption of these active mediators takes place over the non-active anode [38].

According to figure 6, the electrocatalytic performance of electrodes in this work is in the following order: Ti felt/TiO_2 nanotubes/PbO_2 > Ti felt/TiO_2 NTs. This represented the better capability of the substrate decorated with PbO_2 to degrade the dye at higher potential. Oxygen evolution started at given applied potential at a specified scan rate by using different electrodes was due to the anodic reactions reveals with the electroactive and transitional species. An oxygen evolution started at higher potential by using Ti felt/TiO_2 NTs/PbO_2 showed the positive improvement of the substrate by the addition of PbO_2 with subsequent $^{\cdot}OH$ mediated electrocatalytic oxidation of the dye molecules.

The oxygen evolution reaction (OER) is a secondary anodic process. The free radical generated during electrochemical

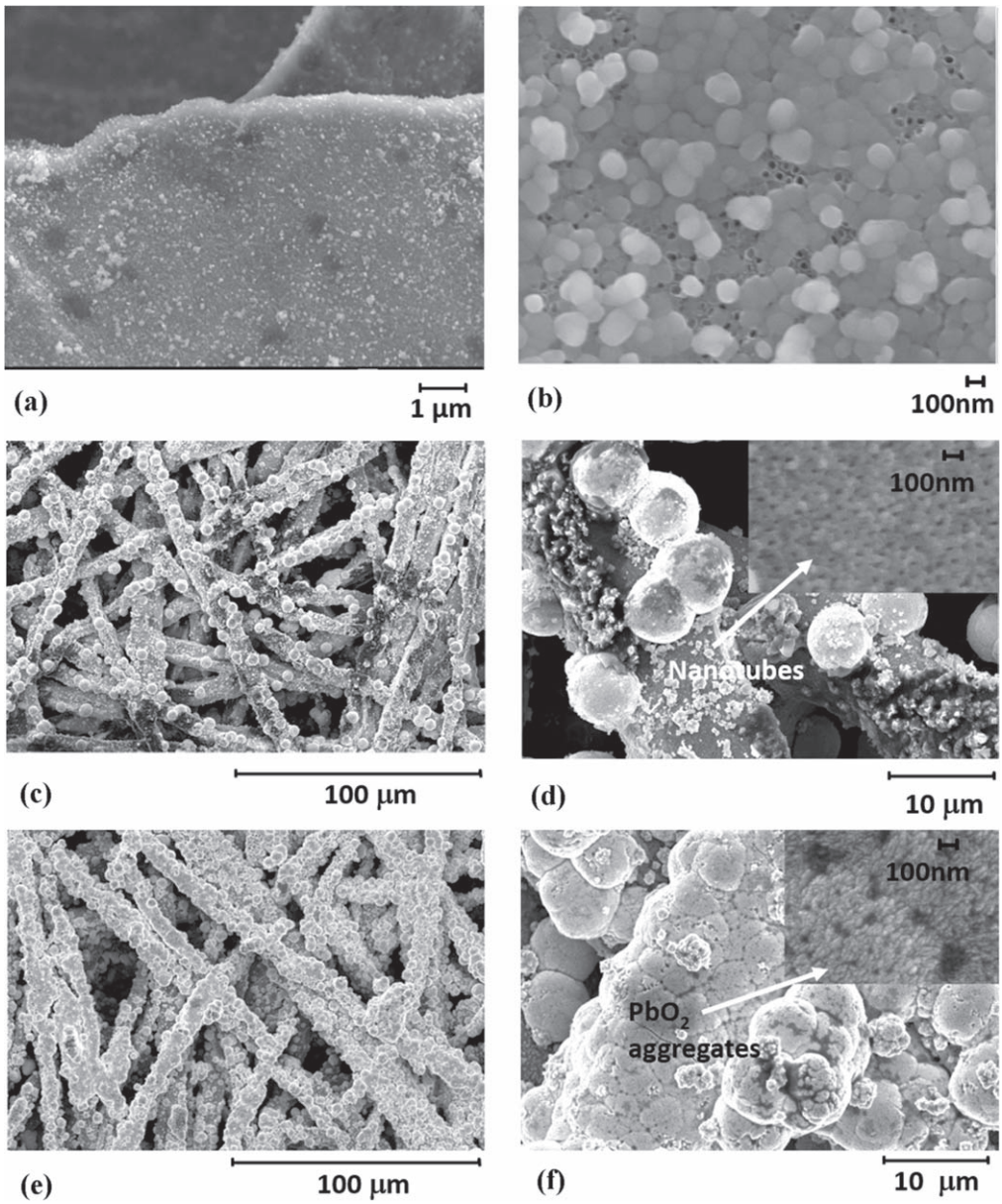

Figure 3. FESEM images of (a) PbO_2 covered TiO_2 NTs ($t_i = 15$ min) on Ti felt; (b) at higher magnification; (c) TiO_2 NTs decorated with PbO_2 ($t_i = 6$ h); (d) microsphere aggregate of PbO_2 crystals ($t_i = 6$ h) on Ti felt, the inset shows the covered nanotubes with PbO_2 NPs; (e) TiO_2 NTs covered by PbO_2 ($t_i = 12$ h) on Ti felt; (f) coalescence of PbO_2 microspheres ($t_i = 12$ h), the inset shows the PbO_2 NPs which aggregated into microspheres.

oxidation of RB-5 dye is the result of intermediate reaction taking place just before the oxygen evolution reaction. The water discharge is the first step during the course of these intermediate reactions which ultimately generate mediated hydroxyl radicals ($^{\cdot}OH$) at the anode. The nature of electrode also plays an important role in the impact of hydroxyl radicals over the anode surface as subsequent steps in anodic oxidation. From the above illustration two types of substrates can be categorised for anodic oxidation: active and non-active electrodes [39]. Active electrodes are strongly influenced by hydroxyl radical interaction with the anode [40]. The interaction of active anodes and hydroxyl radical leads to the formation of higher oxides or superoxides which oxidise the organic while competing with oxygen evolution reaction [39, 40]. Pt is one of the active anodes with high adsorption enthalpies which was extensively studied due to its attracting nature towards hydroxyl radicals. Meanwhile, the hydroxyl radical itself is responsible for the oxidation of organic for non-active electrodes. The decorated PbO_2 NPs over TiO_2 NTs act as a sink for electron removal and have no influence on the anodic oxidation since hydroxyl radicals actively participate in the anodic reaction; PbO_2 can be viewed as a relatively non-active electrode.

3.4. Electrochemical removal and discolouration of RB-5 dye

The colour degradation was studied by electrolysis of electrolyte containing RB-5 dye and using novel coating as anode with applied constant potential at 1.5 V versus Hg/HgO in figure 7. An 80 ml of electrolyte containing 20 ppm of RB-5

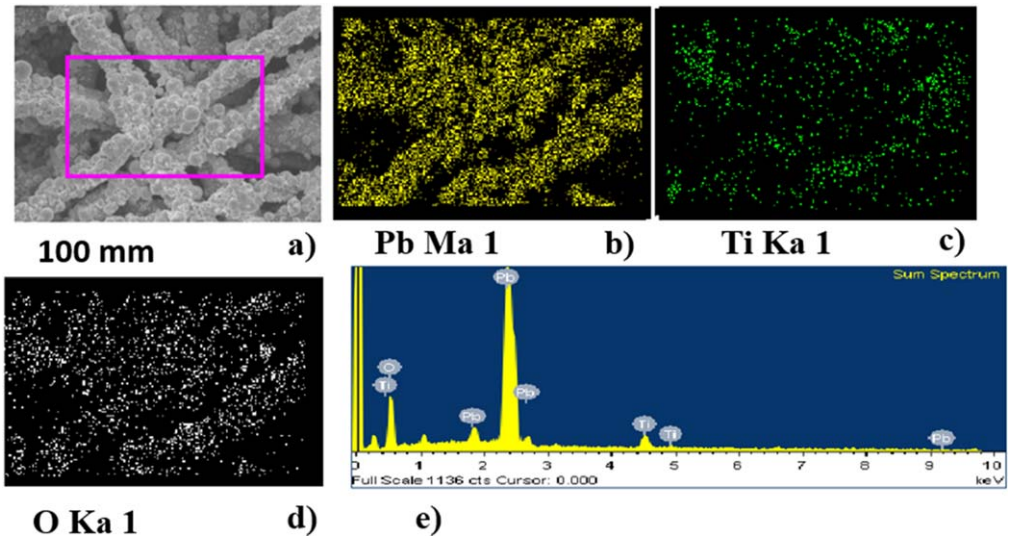

Figure 4. EDX images for elemental analysis of calcined Ti felt/TiO_2 NTs/PbO_2 obtained by anodising and layer by layer immersion: (a) square box shows EDX area of calcined Ti felt/TiO_2 NTs/PbO_2; (b) Pb elemental analysis; (c) Ti elemental analysis; (d) O elemental analysis; (e) sum spectrum for elemental analysis.

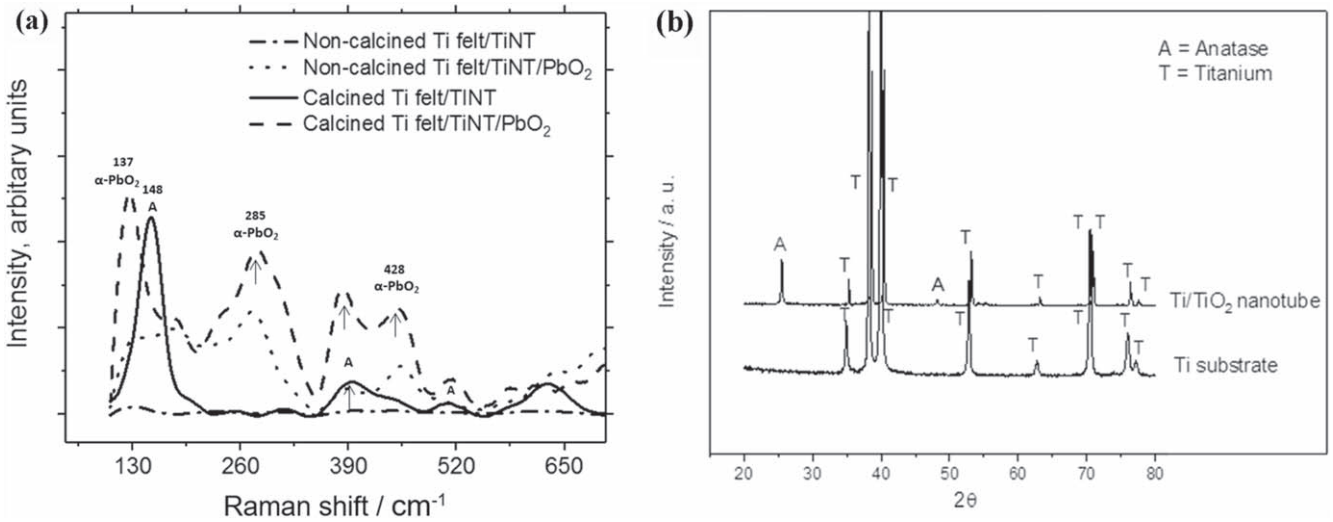

Figure 5. (a) Raman spectra of calcined and non-calcined Ti felt/TiO_2 NTs/PbO_2 as well as Ti felt/TiO_2 NTs; (b) x-ray diffraction of Ti felt and calcined Ti/TiO_2 NTs. A in the graphs denoted peak of anatase.

dye with 0.5 M of Na_2SO_4 at pH 3 was used for electrolysis studies with working electrode (Ti felt/TiO_2 NTs/PbO_2, Ti felt/TiO_2 NTs or Ti felt), counter electrode (Pt) and reference electrode (Hg/HgO (0.6 M NaOH)). The UV-vis spectra measured during constant current electrolysis of the electrolyte for the maximum absorbance band for RB-5 dye in the visible region ($\lambda_{max} = 597$ nm) decreased as a function of time. By using calcined Ti felt/TiO_2 NTs/PbO_2 as working electrode, the intensity of visible band was continuously reduced over 60 min of electrolysis (figure 7).

There is no evidence of new bands in the absorbance data, denoting prompt transformation in the dye structure during electrochemical treatment steps which may associate with the oxidation of complex dye structure into elementary molecules (CO_2) [41]. Different elementary aliphatic and aromatic hydrocarbons may arise due to the oxidation of RB-5 dye, this results from the displacement of functional groups (chromophore groups) present in azo dyes and ultimately removal of these groups to carbon dioxide and organic acids (carboxylic acid) [42]. The normalised concentration related to the time for electrolysis studies of dye using Ti felt/TiO_2 NTs/PbO_2, Ti felt/TiO_2 NTs, Ti felt as anode is represented in figure 7. A pseudo-first order decay of the initial concentration of dye, C_o, with time t can be described by:

$$\ln\left(\frac{C}{C_0}\right) = -kt \tag{3}$$

where k is the apparent first order rate constant, C is the dye concentration. A comparison of observed rate constants is given in table 1.

The different values of normalised concentration and pseudo first order removal kinetics are influenced by the

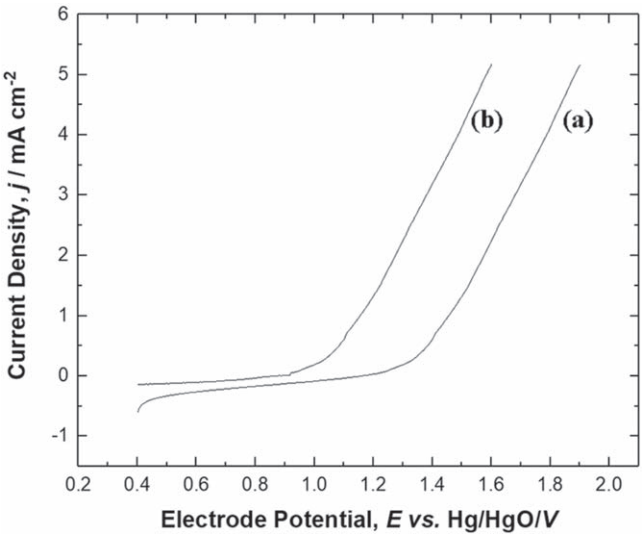

Figure 6. Polarisation curve by using novel coating: (a) Ti felt/TiO_2 NTs/PbO_2 as anode after calcination at 450 °C in an electrolyte containing 20 ppm RB-5 dye in 0.5 M Na_2SO_4 at pH = 3.0; (b) Ti felt/TiO_2 NTs in an electrolyte containing 20 ppm RB-5 dye in 0.5 M Na_2SO_4 background electrolyte, potential sweep rate of 10 mV s^{-1} at 25 °C

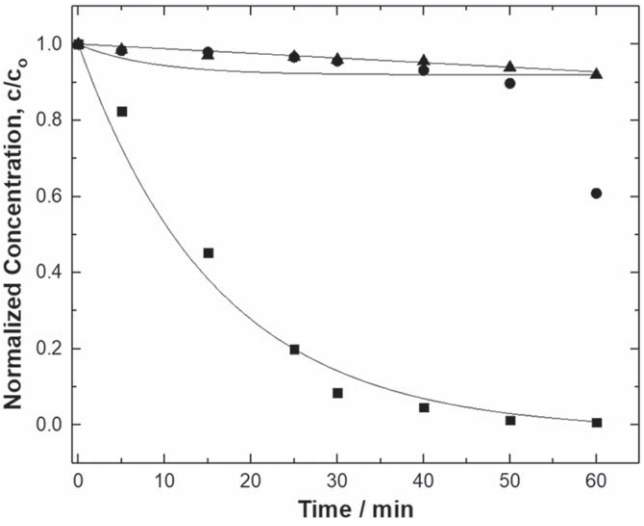

Figure 7. Electrochemical remediation of RB-5 dye by ▲) Ti felt, ●) Ti felt/TiO_2 NTs, and ■) Ti felt/TiO_2 NTs/PbO_2.

electroactive nature of the different substrates used and the architecture of the electrode in which 3D electrode gives more surface area for generation of ·OH radicals. The said performance may arise due to the tendency of Ti felt/TiO_2 NTs/PbO_2 to transform mediated ·OH radicals to oxidised dye or direct attack of hydroxyl radical to the azo dye instead of promoting oxygen evolution.

The polarisation curves are shown in figure 6 for anodic oxidation of RB-5 dye, comparing the performance of two electrodes i.e. Ti felt/TiO_2 NTs/PbO_2 and Ti felt/TiO_2 NTs. The curves show that Ti felt/TiO_2 NTs/PbO_2 exhibited a more efficient colour removal with linear pseudo first order degradation at a controlled potential 1.5 V versus Hg/HgO as seen in figures 7 and 8.

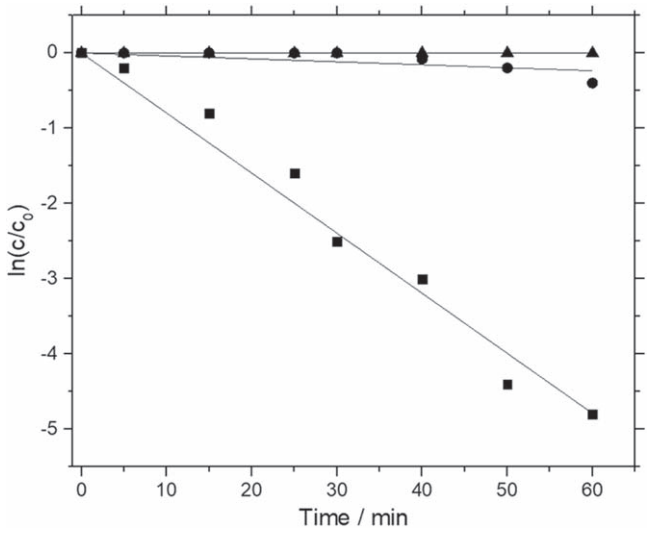

Figure 8. Electrochemical remediation kinetics of RB-5 dye by ▲) T felt, ●) Ti felt/TiO_2 NTs, and ■) Ti felt/TiO_2 NTs/PbO_2.

Water discharge produces ·OH free radical mediators which ultimately lead to colour removal. As almost negligible colour removal (40% after 60 min) was observed for Ti felt/TiO_2 NTs during anodic oxidation which might be due to the adsorption of dye on nanotubes instead of degradation by radicals. Moreover, the lower results for Ti felt alone were observed, with discoloration of dye of about 7% after 60 min which is quite small while comparing with that of calcined Ti felt/TiO_2 NTs/PbO_2 which was about 98% and 99% degradation in 50 and 60 min respectively, showing that the potential gives rise to oxidation of Ti felt. For Ti felt/TiO_2 NTs/PbO_2 the nature of PbO_2 assists generation of physisorbed ·OH radicals as explained by reaction (1) and nanotubes can provide a platform to adsorb the dye molecules inside the tubes present on the Ti felt substrate.

Table 1 shows that the rapid degradation of RB-5 dye with 98% colour removal was seen by using 3D Ti felt/TiO_2 NTs/PbO_2 substrate in about 50 min at constant potential 1.5 V versus Hg/HgO. The calculated rate constant at this constant potential is 0.0875 min^{-1}. The lowest apparent rate constant was seen at titanium felt, approximately 0.0012 min^{-1}. It is 10 times lower than the rate for anodic oxidation of RB-5 dye using the Ti felt/TiO_2 NTs/PbO_2 substrate. The rate constant for Ti felt/TiO_2 NTs was found to be 0.0058 min^{-1} as dye molecules adsorbed over surface site of negatively charged nanotubes [43].

This hierarchical modification of surfaces could be applied for 3D printed electrode for future work. Several surface pre-treatments, fluid flow, and heat transfer, which may alter diffusion-controlled growth and coalescence [44], are interesting to be studied.

4. Conclusions

TiO_2 NTs can be formed on the top surface of titanium felt with nanotubular arrangements using MSA (1 M) containing ammonium fluoride 1.0 wt.% by anodising at an applied cell

potential of 10 V for small nanotubes (diameter ~50 nm) and 20 V for large nanotubes (diameter ~100 nm). The PbO_2 can be deposited inside the nanotubes by immersion of anodised titanium felt and hydrothermal treatment in a solution containing $Pb(NO_3)_2$ and structure directing agent (PVP). The immersion time (t_i) plays an important role in the deposition of PbO_2 over nanotubular structures following LaMer-Dinegar theory which started with rapid nucleation, followed by mesoscale formation and coalescence of PbO_2 microsphere aggregates. Further application of these coatings showed that Ti felt/TiO_2 NTs/PbO_2 exhibited the electrochemical dye discoloration of about 99% in 60 min at 1.5 V versus Hg/HgO. The electrochemical performance of coating was improved by the presence of PbO_2 as a non-active anode capable of mediating the electrogeneration of hydroxyl radical during water discharge. This research points the way to a practical approach to decorate metal oxide structures on TiO_2 NTs over inexpensive porous 3D Ti-felt substrate, for environmental remediation of wastewater.

Acknowledgments

S Z J Zaidi is grateful to the Faculty of Engineering and the Environment at the University of Southampton for the Rayleigh studentship, to the Bestway Foundation, Charity No. 297178, UK and to the European Commission Project H2020 CO2EXIDE, for the economic support.

Conflict of interest

The authors declare that they have no conflict of interest.

References

[1] Mai T T T, Phan T B, Pham T T and Vu H H 2014 *Adv. Nat. Sci. Nanosci. Nanotechnol.* **5** 025004
[2] Martins A S, Harito C, Bavykin D V, Walsh F C and Lanza M R V 2017 *J. Mater. Chem.* C **5** 3955
[3] Fang M, Dong G, Wei R and Ho J C 2017 *Adv. Energy Mater.* **7** 1700559
[4] Souza J S, Carvalho W M, Souza F L, Ponce-De-Leon C, Bavykin D V and Alves W A 2016 *J. Mater. Chem.* A **4** 944
[5] Arenas L F, Ponce de León C and Walsh F C 2019 *Curr. Opin. Electrochem.* **16** 1
[6] Jermy B R and Ravinayagam V 2019 *Adv. Nat. Sci. Nanosci. Nanotechnol.* **10** 045003
[7] Arenas L F, Ponce de León C, Boardman R P and Walsh F C 2017 *J. Electrochem. Soc.* **164** D57–66
[8] Calatayud D G, Martin R F, Castellanos-Aliaga A, Peiteado M, Simon F J P, Caballero A and Jardiel T 2020 *Nanotechnology* **31** 045603
[9] Harito C, Porras R, Bavykin D V and Walsh F C 2017 *J. Appl. Polym. Sci.* **134** 44641
[10] Harito C, Bavykin D V, Yuliarto B, Dipojono H K and Walsh F C 2019 *J. Polym. Environ.* **27** 1505
[11] Tri W W, Riza P B, Harito C, Bavykin D V, Walsh F C, James T D, Kociok-Köhn G and Marken F 2018 *Electroanalysis* **30** 1303
[12] Wahyuni W T, Putra B R, Harito C, Bavykin D V, Walsh F C, Fletcher P J and Marken F 2019 *Anal. Chim. Acta* X **1** 100001
[13] Vu T T T, Le T K A, Nguyen H N, Phan K S, Do H D, Le T T H, Mac N B, Dang D K and Ha P T 2019 *Adv. Nat. Sci. Nanosci. Nanotechnol.* **10** 015010
[14] Putra B R *et al* 2019 *J. Solid State Electrochem.* **23** 1237
[15] Dubey P K, Kumar R, Pandey A C, Tiwari R S and Srivastava O N 2017 *Int. J. Hydrogen Energy* **42** 4782
[16] Dubey P K, Kumar R, Tiwari R S, Srivastava O N, Pandey A C and Singh P 2018 *Int. J. Hydrogen Energy* **43** 6867
[17] An H, Cui H, Zhang W, Zhai J, Qian Y, Xie X and Li Q 2012 *Chem. Eng. J.* **209** 86
[18] Li X, Pletcher D and Walsh F C 2011 *Chem. Soc. Rev.* **40** 3879
[19] Thomas U B 1948 *J. Electrochem. Soc.* **94** 42
[20] Wielewski L P, Zuccolotto T, Soares M, Prola L D T and de Liz M V 2020 *Rev. Ambient. Água* **15** e2464
[21] Bavykin D V and Walsh F C 2009 *Titanate and Titania Nanotubes* (Cambridge: Royal Society of Chemistry)
[22] Low C T J, De La Toba Corral M and Walsh F C 2011 *Trans. Inst. Met. Finish.* **89** 44
[23] Mor G K, Varghese O K, Paulose M, Shankar K and Grimes C A 2006 *Sol. Energy Mater. Sol. Cells* **90** 2011
[24] Macak J M, Tsuchiya H, Ghicov A, Yasuda K, Hahn R, Bauer S and Schmuki P 2007 *Curr. Opin. Solid State Mater. Sci.* **11** 3
[25] Mor G K, Varghese O K, Paulose M, Mukherjee N and Grimes C A 2003 *J. Mater. Res.* **18** 2588
[26] Kunze J, Seyeux A and Schmuki P 2008 *Electrochem. Solid-State Lett.* **11** K11
[27] Xu H, Zhang Q, Yan W, Chu W and Zhang L 2013 *Int. J. Electrochem. Sci.* **8** 5382
[28] Moura D C D, Quiroz M A, Silva D R D, Salazar R and Martínez-Huitle C A 2016 *Environ. Nanotechnology Monit. Manag.* **5** 13
[29] Elaissaoui I, Akrout H and Bousselmi L 2016 *Desalin. Water Treat.* **57** 22120
[30] Zaidi S Z J, Harito C, Walsh F C and Ponce de León C 2018 *J. Solid State Electrochem.* **22** 2889
[31] Ghasemi S, Karami H and Khanezar H 2014 *J. Mater. Sci.* **49** 1014
[32] Lamer V K and Dinegar R H 1950 *J. Am. Chem. Soc.* **72** 4847
[33] Bahrig L, Hickey S G and Eychmüller A 2014 *Cryst. Eng. Comm.* **16** 9408
[34] Hu H, Singh M, Wan X, Tang J, Chu C W and Li G 2020 *J. Mater. Chem.* A **8** 1578
[35] Burgio L, Clark R J H and Firth S 2001 *Analyst* **126** 222
[36] Nguyen T L, Ung T D T and Nguyen Q L 2014 *Adv. Nat. Sci. Nanosci. Nanotechnol.* **5** 025016
[37] Kim C, Kim S, Hong S P, Lee J and Yoon J 2016 *Phys. Chem. Chem. Phys.* **18** 14370
[38] dos Santos A J, de Souza Xavier D K, da Silva D R, Quiroz M A and Martínez-Huitle C A 2014 *J. Mex. Chem. Soc.* **58** 356
[39] Martínez-Huitle C A and Brillas E 2009 *Appl. Catal. B Environ.* **87** 105
[40] Sirés I, Brillas E, Oturan M A, Rodrigo M A and Panizza M 2014 *Environ. Sci. Pollut. Res.* **21** 8336
[41] Martínez-Huitle C A and Ferro S 2006 *Chem. Soc. Rev.* **35** 1324
[42] De Oliveira G R, Fernandes N S, Melo J V, de Da Silva D R, Urgeghe C and Martínez-Huitle C A 2011 *Chem. Eng. J.* **168** 208
[43] Shen Y, Wang W and Xiao K 2016 *J. Environ. Chem. Eng.* **4** 1259
[44] Walsh F C, Arenas L F and Ponce de León C 2020 *Trans. IMF* **98** 65